Article

Journal of
Nanoscience and Nanotechnology
Vol. 19, 2008–2015, 2019
www.aspbs.com/jnn

Electrochemical Synthesis and Magnetic Properties of MFe_2O_4 (M = Fe, Mn, Co, Ni) Nanoparticles for Potential Biomedical Applications

J. G. Ovejero[1,2], A. Mayoral[3], M. Cañete[4], M. García[1,5], A. Hernando[1], and P. Herrasti[2,*]

[1] *Instituto de Magnetismo Aplicado, 'Salvador Velayos', UCM-CSIC-ADIF, Las Rozas, P.O. Box 155, Madrid 28230, Spain*
[2] *Departamento de Química Física Aplicada, Facultad de Ciencias, Universidad Autónoma de Madrid, Cantoblanco s/n, 28049 Madrid, Spain*
[3] *Laboratorio de Microscopias Avanzadas (LMA), Instituto de Nanociencia de Aragón, Universidad de Zaragoza, Mariano Esquillor s/n, 50018 Zaragoza, Spain*
[4] *Departamento de Biología, Facultad de Ciencias, Universidad Autónoma de Madrid, Cantoblanco s/n, 28049 Madrid, Spain*
[5] *Instituto de Cerámica y Vidrio, ICV-CSIC, Cantoblanco, C/Kelsen, 5, 28049 Madrid, Spain*

In this study, we evaluate the magnetic properties and cytotoxic effect of magnetic nanoparticles (MNPs) based on magnetite and Mn, Co and Ni ferrites, obtained by electrochemical synthesis. These nanoparticles have almost spherical shape and an mode size of 9 ± 1 nm. The electrochemical synthesis produces a single crystallographic phase with a spinel-like structure in all cases. Magnetization saturation at room temperature varies with the composition of the ferrites from M_S (Fe_3O_4) > M_S ($MnFe_2O_4$) > M_S ($CoFe_2O_4$) > M_S ($NiFe_2O_4$). Ferrite MNPs present low magnetic remanence indicating a superparamagnetic-like response at room temperature. However, the different values of magnetic anisotropy and size produce variations in the values of coercivity and susceptibility of the ferrite MNPs. The cytotoxicity of the different ferrites was evaluated by internalizing MNP in HeLa cancer cells. Although magnetite and Mn ferrite present low toxicity for all the concentrations studied, significant cytotoxic effect were observed when incubating the cells with high concentration of Co and Ni ferrites.

Keywords: Electrosynthesis, Ferrites Nanoparticles, Internalization, Magnetic Properties.

1. INTRODUCTION

Nanoparticles represents an important field of study in the actual nanotechnology research.[1] They are commonly defined as materials with sizes smaller that 100 nm in their three spatial directions. Magnetic nanoparticles (MNPs) are a special kind of nanoparticle that in recent years have attracted the attention of many research groups across the world. Their strong response to external magnetic fields, combined with their small size, opens up a whole bunch of possible applications such as: catalysis,[2,3] waste water treatment,[4–6] data storage (electronics)[7,8] and several applications in the field of medicine, some examples are: targeted hyperthermia,[9–11] drug delivery,[12,13] MRI contrast agents[14] and biosensors.[15]

The main challenge in magnetic nanoparticle synthesis consists on finding a specific set of experimental conditions that yield a material with high crystallinity, narrow size distribution and little to no secondary species (high purity). In order to fulfill these requirements, a great deal of effort has been put towards investigating a wide variety of approaches to produce nanometric materials. The choice of the synthesis method greatly influence the physical and chemical properties of the MNP. Because of that, new approaches are currently being studied profoundly.[16]

Among the rapidly growing number of techniques used for the production of MNPs, the electrochemical methods offer attractive features and advantages over some of their counterparts. For example, they produce a clean product with a well-controlled nanoparticle size, in the order of 10 to 30 nm, a narrow size distribution plus excellent magnetic properties, these features results desirable for biomedical applications such as hyperthermia for cancer treatment.[17] In addition, they are suitable for scaling-up production by enlarging size and number of electrodes, varying current density, assembling a

*Author to whom correspondence should be addressed.

 1533-4880/2019/19/2008/008 doi:10.1166/jnn.2019.15313

continuous electrochemical cell process or by combining some of these approaches.[18, 19]

The electrochemical synthesis of magnetite nanoparticles is a relatively simple methodology that consists in passing an electric current between 2 Fe electrodes. As one of the electrodes acts as anode, it electrochemically dissolves and produces ionic Fe species. On the surface of the other electrode (cathode) the reduction of water takes place, which produces both hydroxyl ions and H_2 gas. As simple as the technique may sound, the main characteristics of magnetite nanoparticles, such as morphology, structure, size and size distribution are highly dependent on the electrochemical cell geometry and operating conditions such as: electrode separation, current density, applied cell potential, temperature, stirring and electrolyte composition.[18, 19] Variations on these parameters, can change not just the size and shape of the MNPs, but also the crystal structure and magnetic properties.[20]

Another significant advantage of electrochemical synthesis is the possibility of producing binary or ternary ferrites by including in the reaction electrodes of different metals.[17, 21] However, a careful control of the synthesis parameter must be undertaken in order to produce single phase nanoparticles avoiding hidroxydes impurities or polycrystalline MNPs.

Features such as the average size, the shape and the composition of the MNPs must be carefully characterized to evaluate the magnetic properties of individual MNPs. Furthermore, in a magnetic colloid composed by many MNPs, the contributions of both finite size effects and interparticle interactions must be taken into account too.[22]

On the other side, the application of electrochemically synthesized MNP to biological systems requires a careful viability assay that studies the cytotoxic effect of these materials in human cell lines.[23]

In this work we have prepared different ferrite MNPs containing Fe, Co, Mn and Ni by electrochemical synthesis. The synthesis parameters have been varied to obtain ferrite MNP with a similar mode size and a chemical composition close to the stoichiometry. After being synthesized, the MNPs were functionalized with citric acid. Their magnetic and structural properties have been studied as well as their suitability for biomedical applications through assays of internalization and cytotoxicity in HeLa cells.

2. EXPERIMENTAL DETAILS

Electrochemical synthesis based on previous works[15, 18, 21, 24] was employed to synthesize MNPs of magnetite, and Mn, Ni and Co ferrites. In the case of magnetite, the synthesis was carried out with a system of two flat Fe electrodes of 2 cm^2 and 8 cm^2 acting as an anode and cathode, respectively. For the synthesis of ferrites a three electrodes system was employed. It was composed by two flat anodes (Fe and M, M = Co, Ni and Mn) and a cylindrical cathode of Fe that surround both anodes. The size of the electrodes was 2 cm^2 for both anodes and 90 cm^2 for cathode.

The time for the electrosynthesis was fixed to 30 min in all cases and the temperature was set to 5 °C using a thermalized glass. The electrolyte (Tetrabutylammonium bromide 0.04 M) was vigorously stirred using magnetic agitation. The current density applied to the electrodes was varied with the aim to obtain MNPs of similar size and composition. Magnetite MNPs were prepared with a current density of 45 mA/cm^2. In the case of the ferrite MNP, the current density of the Fe anode was kept as 45 mA/cm^2 and the current density of the second anode was set to 45 mA/cm^2, 40 mA/cm^2, 25 mA/cm^2 for Ni, Mn and Co ferrite, respectively.[15, 17, 21]

After 30 min, the current was stopped and the electrodes were extracted from the medium. The MNPs were then precipitated by magnetic decantation using a neodymium magnet (0.6 T) and the medium was replaced by distilled water for the removal of non-magnetic by-products from the reaction. This process was repeated 3 times.

The MNP were functionalized with citric acid by dissolving 50 mg of this molecule in the colloids. After dissolving the citric acid, the pH of the reaction was adjusted to pH = 5 using a diluted solution of KOH and heated up to 80 °C for 2 hours with a vigorous magnetic stirring. At the end of the coating process, the MNP were washed by triple magnetic decantation for three times. To evaluate the structural and magnetic properties, samples were dried to powders by lyophilizing a concentrated colloid of MNPs for 24 hours.

The size, shape and crystallographic structure of the samples were studied by depositing a diluted colloid of MNP over a Cu grid. Low magnification transmission electron microscopy (TEM) pictures were obtained with a JEM 1400 (JEOL) equipped with energy-dispersive X-ray (EDX) spectrometer. In the case of high resolution TEM images (HRTEM), it was employed a TITAN scanning transmission electron microscope (STEM, FEI Company) with a high angle annular dark field (HAADF) detector and electron energy loss spectrometer (EELS).

The crystallinity of the MNP powders was evaluated using a X'pert MPD X-ray difractometer (Philips) with 0,03° step and an acquisition time of 3 s/step. The compositional stoichiometry and the colloid concentration were measured with an inductively coupled plasma-optical emission spectrometer (ICP-OES) Perkin Elmer Optima 2100DV. The magnetic properties were measured with an SQUID magnetometer MPMS XL-5 (Quantum Design). The Zero Field Cooling-Field Cooling curves (ZFCFC) were obtained cooling down the sample to 10 K with and without an applied field of 100 Oe and measuring the susceptibility (χ) while heating up with the same applied field.

The biological effects of the MNPs were tested using human carcinoma HeLa cells. A series of 24 well plates containing an identical number of cells were incubated

during 24 h with different MNPs concentrations. Then, the cells of the first column of the plate (1X4)-prepared over coverslips—were fixed in cold ethanol (5 min) and stained with methylene blue (T_B: 0.05 mg/ml distilled water, 0.5 min) for internalization studies.

The viability of the cells was analyzed by the 3-(4,5-dimethyl-thiazol-2-yl)-2,5-diphenyltetrazolium (MTT) colorimetric assay using the rest of the columns of the plate. A day after incubation, the medium was removed and substituted by new medium mixed with MTT at a final concentration of 0.05 mg/ml. After 4 h of incubation the medium was discarded and water non-soluble formazan crystals were dissolved in 500 μl of DMSO, added to each well. Considering that the MNPs absorption could affect the results, DMSO solutions were centrifuged (10000 rpm, 15 min) and transferred to a clean new plate before evaluation. The optical density was measured in a Tecan Spectra Fluor spectrophotometer microplate reader at 540 nm. Cell survival was expressed as the percentage of absorption of treated cells relative to control cells. The mean value and standard deviation from at least 5 experiments were obtained.

3. RESULTS AND DISCUSSION

Figure 1 shows the TEM micrographs of the ferrite MNPs obtained by electrochemical synthesis. The MNPs electrosynthesized have a nearly spherical geometry with a mode size of 9 ± 1 nm. However, the dispersity of the sample implies that the average size of the MNPs varies between 9 and 14 nm with standard deviations over 0.35. Using this synthesis route is possible to produce water-dispersed MNP of larger size than other techniques, in a simple way and avoiding organic solvents.

To verify the chemical composition of the samples, an elemental analysis of EDX was performed. The spectra obtained, show two common peaks in 6.4 KeV and 7.1 KeV attributable to the K_α and K_β emission of Fe. Additional peaks at 5.9, 7.7 and 7.4 KeV in the (f), (i) and (l) spectra corresponds to the K_α transitions of Mn and K_β transitions of Co and Ni, respectively. The rest of the EDX emissions appear overlapped with other peaks and result unclear. The Cu and Cr peaks must be attributed to the sample holder.

The X-ray diffraction patterns in Figure 2(a) show that the electrochemical synthesis of MNPs produces a single

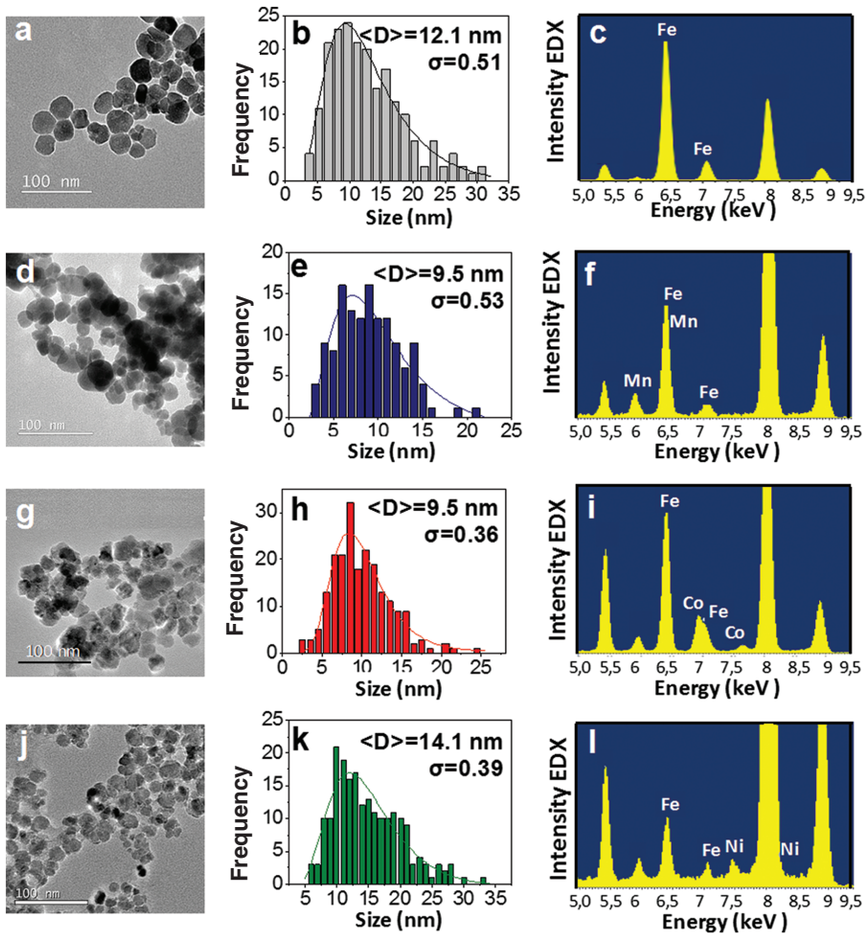

Figure 1. TEM images of the NPMs synthesized for the different ferrites: (a) Fe, (d) Mn, (g) Co and (j) Ni. Sizes distribution: (b) Fe, (e) Mn, (h) Co and (k) Ni. EDX spectra obtained by the different ferrites: (c) Fe, (f) Mn, (i) Co and (l) Ni.

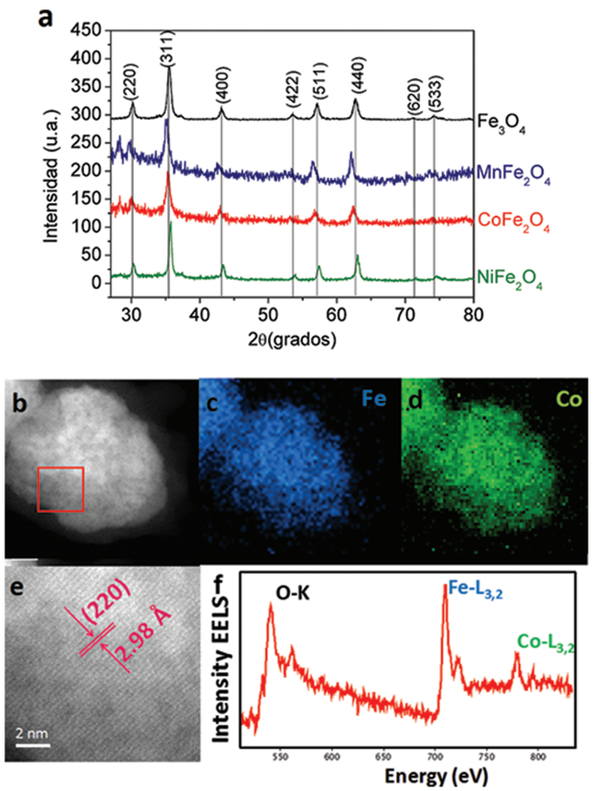

Figure 2. (a) X-ray diffraction pattern of the synthesized ferrites. (b) STEM-HAADF image of a Co ferrite MNP. Compositional mapping obtained by EELS from (c) Fe and (d) Co on the image shown in (b). (e) Enlarging the red square of the image shown in (b). EELS spectrum for the identification of the peaks associated to the transition K of O and the transition $L_{3,2}$ of Fe and Co.

crystallographic phase with a spinel-like structure. The associated crystallographic direction is indicated on each refraction peak. By adjusting the spectra using a Rietveld refinement, both the crystal size and the lattice parameter were obtained. The Table I collects the values resulting from these adjustments. The substitution of one of the Fe ions of the magnetite by another transition metal produces variations of hundredths of Å in the (311) crystal spacing.

Table I. Values obtained for the different ferrites of: Crystal size according to the formula of Scherrer ($D_{Scherrer}$) and interatomic distance obtained from 311 peak of the X-ray diffractograms (a_{311}); concentration of Fe ($[Fe_{ICP\text{-}OES}]$) and the ion corresponding to each ferrite ($[X_{ICP\text{-}OES}]$) obtained by ICP-OES; and proportion of the substitution ions of each of the ferrites ($[X]_{ICP\text{-}OES}/[Fe]_{ICP\text{-}OES}$).

	Magnetite	Mn ferrite (X = Mn)	Co ferrite (X = Co)	Ni ferrite (X = Ni)
$D_{Scherrer}$ (nm)	13.1	9.9	7.8	12.2
$a_{(311)}$ (Å)	2.52	2.55	2.54	2.52
$[Fe]_{ICP\text{-}OES}$	1.315	1.194	0.312	1.244
$[X]_{ICP\text{-}OES}$	–	0.367	0.125	0.558
$M_xFe_{3-x}O_4$	Fe_3O_4	$M_{0.7}Fe_{2.3}O_4$	$M_{0.9}Fe_{2.1}O_4$	$M_{0.9}Fe_{2.1}O_4$

As example, Figures 2(b)–(d) show the HRTEM-HAADF images of a Co ferrite MNP together with its corresponding compositional analysis by EELS. This set of images display the distribution of each element in the ferrites. From the mapping performed for the Fe and Co signals, the distribution for both elements results to be homogeneous throughout the whole volume, without sign of species segregation in the MNP. Such homogeneity in registered signal suggest that both atoms are well distributed in the spinel crystalline lattice.

Figure 2(e) shows an enlargement of the region in red on Figure 2(b). It shows an interplanar spacing of 2.93 Å corresponding to the direction (220) of the spinel ferrites. The sequence of periodic planes is observed throughout the volume of the NP, which supports the good crystallinity of the nanoparticles. Figure 2(f) shows the energy loss spectrum of the electrons with the Fe and Co peaks corresponding to their $L_{3,2}$ transitions that were selected for compositional mapping. The relative intensity of the signals recorded for Fe and Co is in agreement with the 2:1 ratio of the stoichiometric ferrites.

To confirm the proportion of metal ions in the different ferrites, samples were digested with aqua regia in a controlled volume and analyzed by ICP-OES. This technique measures the amount of metal ions per unit volume and the proportion between them. As a result, both the magnetic material concentration and the stoichiometry of the ferrite MNPs could be calculated. Table I shows the results obtained by this technique. In view of the results, we can conclude that, using the proper electric currents, is possible to synthesize ferrite MNPs with compositions very close to stoichiometric. This is important when comparing the effect of cation substitution in the magnetic properties of the different ferrites.

Figure 3 shows the M–H hysteresis loops of the Fe oxide NPM (black) and the Mn (blue), Co (red) and Ni (green) ferrites measured in powder form. We clearly observe that the magnetization and coercivity of the cycles are modified by replacing the Fe ions in the crystal lattice with other elements of the 3*d* group with different Bohr magnetons and exchange interactions.[25, 26]

In the cycles measured at 10 K the saturation magnetization of the MNP follows a progression similar to that observed in their bulk materials: M_S ($MnFe_2O_4$) > M_S (Fe_3O_4) > M_S ($CoFe_2O_4$) > M_S ($NiFe_2O_4$).[25] On the other hand, at room temperature, this order is altered. In the smaller NPs ($MnFe_2O_4$ and $CoFe_2O_4$), a higher magnetization loss occurs, reaching values such as those shown in Table II.

In massive materials the saturation magnetization decays with the temperature following Bloch's law, due to the thermal agitation of the spins. However, it has been observed that in the case of MNPs the greater disorder of the surface spins (spin canting) leads to an extra loss of the magnetization that results more important for smaller MNP.

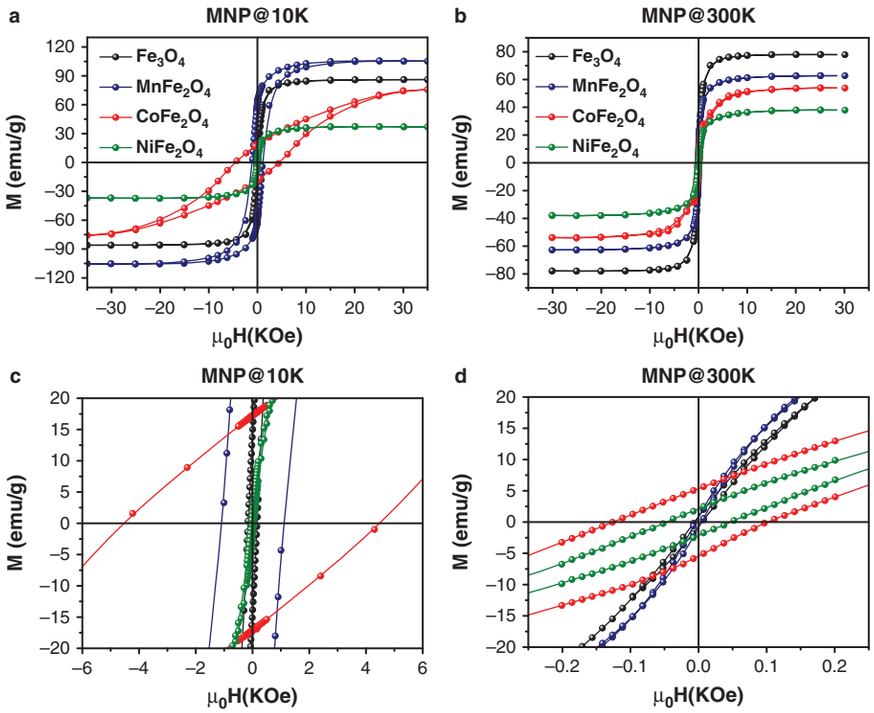

Figure 3. M–H hysteresis loops of different ferrites at 10 K and 300 K: Fe_3O_4 in black, $MnFe_2O_4$ in blue, $CoFe_2O_4$ in red and $NiFe_2O_4$ in green.

Figures 3(c) and (d) show the central zone of the loops and allow us to observe that, although all ferrites present low remanence due to their superparamagnetic character, the different size and composition of the ferrites produce variations in the values of coercivity and susceptibility (χ) of the cycle, as a consequence of their different magnetic anisotropy energies.

Mn ferrite, for example, being a magnetically soft material ($K_{1Bulk} = -3$ KJ/m^3), presents a coercivity value at ambient temperature that is within the experimental error of the measurement and thus can be considered null. The low magnetic anisotropy implies higher χ than the rest of the ferrites. We observed that in the low fields (100 Oe–300 Oe), Mn ferrite reaches the highest value of the magnetization. High χ at low fields can result very useful in biomedical applications such as hyperthermia or MRI.

Table II. Magnetic parameters of the different ferrites.

	Fe_3O_4	$Mn_{0.7}Fe_{2.3}O_4$	$Co_{0.9}Fe_{2.1}O_4$	$Ni_{0.9}Fe_{2.1}O_4$
M_S (emu g^{-1})	77.6	63	54	38
H_c (Oe)	35	5	115	45
χ (memu g^{-1} Oe^{-1})	93	105	39	36
$T_{B,\max}$ (K)	≤10	≤10	290	160
$T_{ZFC,\max}$ (K)	300	280	>300 (340)	>300 (320)
K_{dist} (J m^{-3})	7	10	255	50
K_{ZFC} (J m^{-3})	112	27	261	75
$\lvert K_{1bib}\rvert$ (KJ m^{-3})	13	3	290	7

Notes: M_S: Saturation magnetization at 300 K. H_c: Coercitivity at 300 K. χ: Susceptibility at 300 K measured at 100 Oe. $T_{B,\max}$: Maximum blocking temperature. $T_{ZFC,\max}$: ZFC curve maximum. K_{dist}: Anisotropy constant obtained by T_B distribution. K_{ZFC}: Anisotropy constant obtained from $T_{ZFC,\max}$. $\lvert K_{1bib}\rvert$: Anisotropy collected from the Ref. [28].

The magnetite sample is the one with the highest magnetization value in saturation, 76 emu/g. Although, at low fields (<300 Oe) its χ value is lower than that of the Mn ferrite. For this reason, the suitability of these particles will depend to a large extent on the intensity of the applied field. The coercivity of the sample can still be considered almost null although its value is slightly higher.

In the case of Ni ferrite, despite having a magnetocrystalline anisotropy value similar to magnetite, M–H loops appear open and their coercivity cannot be neglected (Table II). The larger volume of the Ni ferrite implies that the value of the anisotropy energy ($K_V V$) is higher and the magnetic moment of the sample is blocked at room temperature. Its low magnetization value means that the χ of the Ni ferrites is reduced by half with respect to the value of the magnetite.

The Co ferrite is the hardest of the magnetic materials studied, with magnetocrystalline anisotropy values an order of magnitude above the rest of the ferrites. Therefore, though the size of the MNPs is relatively small, the coercivity of their hysteresis cycle remains considerable at room temperature. The Co ferrite, due to its high anisotropy, is the most distant of the superparamagnetic state. As in the case of Ni ferrite, its low magnetization value implies a low χ value.

Figure 4 shows the curves obtained for each ferrite according to the color code used in the M–H hysteresis

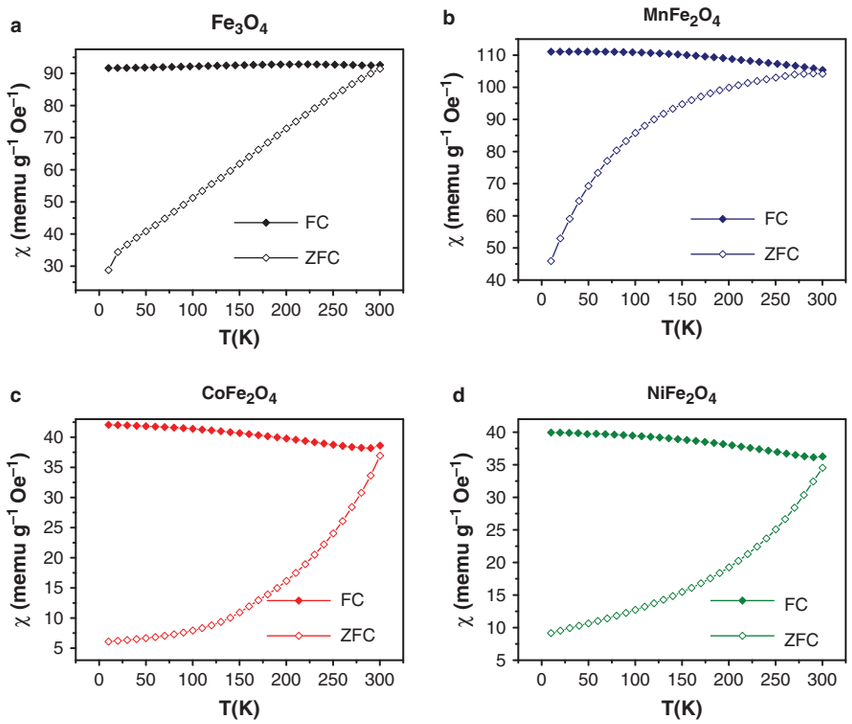

Figure 4. ZFC and FC susceptibility curves for: Fe_3O_4 in black, $MnFe_2O_4$ in blue, $CoFe_2O_4$ in red and $NiFe_2O_4$ in green.

loops. In these graphs, we observe how the χ values of the FC curves decays of around 5% when going from 10 K to 300 K, except in the case of the magnetite in which hardly registered variation. These changes of χ with the temperature agree with those observed in the saturation magnetization of M–H cycles at 10 K and 300 K.

It is also observed that the intersection of the ZFC and FC curves are close to the room temperature confirming the transition to the superparamagnetic state. Table II shows the different temperatures registered for the maximum χ of the ZFC curve ($T_{ZFC,\,max}$).

Although some authors define the blocking temperature (T_B) as the $T_{ZFC,\,max}$, in a polydisperse population of MNPs, the T_B cannot be defined as a single value but must be treated as a distribution of T_B that depends on the volume of the NPMs.

Assuming a single magnetocrystalline anisotropy for all MNPs, the T_B distribution can be related to the size distribution of the sample as expressed in Eq. (1):[27]

$$25K_B\int_0^\infty f(T_B)\,dT = K_V\int_0^\infty f'(V)\,dV \qquad (1)$$

Where $f(T_B)$ is the distribution function of T_B, and $f'(V)$ is the volume distributions of MNPs measured by TEM, K_B is the Boltzman constant and K_V is the magneto-crystalline anisotropy constant of the material. Thus, by determining the distributions $f(T_B)$ and $f'(V)$ of the MNPs, it is possible to find the anisotropy constant that relate each other.

The distribution $f(T_B)$ can be estimated from de ZFCFC curves, by deriving the difference between the ZFC and FC susceptibility curves respect to the temperature, as indicates Eq. (2):[27]

$$f(T_B(T)) \propto \frac{d(\chi_{ZFC}(T)-\chi_{FC}(T))}{dT} \qquad (2)$$

Figure 5 presents the amount of blocked MNPs respect to the temperature for each ferrite. The T_B distributions shown in these histograms were adjusted to a log-normal curve (orange) and compared to the size distribution obtained by TEM, in order to calculate the anisotropy constant that relates each other (K_{dist}). The crystal sizes included in upper axis of the Figure 5 were calculated by substituting T values in Eq. (1). Thus, the crystal size values scales differently depending on the K_{dist} obtained in each ferrite.

It is possible to observe that, as the anisotropy of the material increases, the maximum value of the T_B distribution shifts to higher temperatures, going above room temperature for the Co ferrite MNPs.

For comparison proposes, the value of the anisotropy constant calculated by T_B distribution method was compared to the value obtained from Eq. (3) (K_{ZFC}), where T_B is assumed to be equal to $T_{ZFC,\,max}$ and R is the average radius of the MNPs in TEM:

$$K_{ZFC} = \frac{75K_B}{4\pi}\frac{T_B}{R^3} \qquad (3)$$

Table II summarize the magnetocrystalline anisotropy values estimated from the distributions (K_{dist}), those

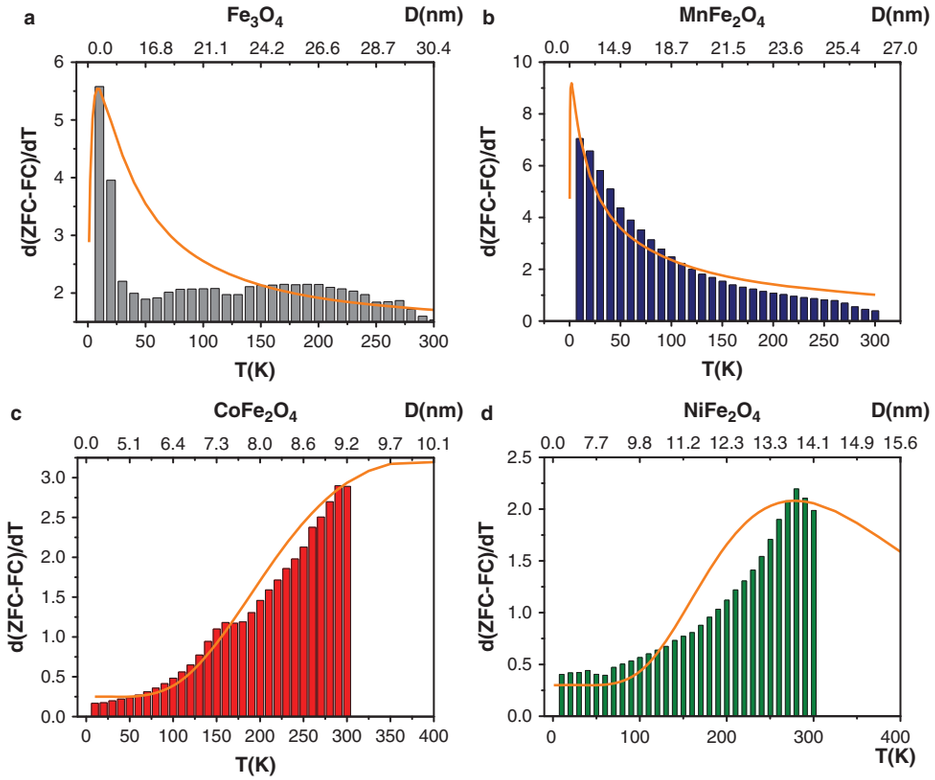

Figure 5. Distribution of T_B with temperature calculated from the ZFCFC susceptibility curves in Figure 4.

calculated from the $T_{ZFC,\,max}$ (K_{ZFC}), and the values reported for the massive materials can be compared. It is possible to observe that, when the distribution of blocking temperatures is taken into account, the anisotropy constant estimated from T_B results closer to the values reported for bulk materials.[28]

In spite of this, the calculated anisotropy values do not fit exactly with reported bulk values. The lack of stoichiometry of the ferrites or the anisotropy associated with the non-sphericity could explain such discrepancy.[29] Also, the magnetic dipolar interactions between MNPs in the form of powder introduce a strong contribution to the anisotropy barriers that results in a displacement of blocking temperatures.[30]

In order to enhance their colloidal stability and promote the internalization of this kind of MNPs in HeLa cells they were coated with citric acid. Figure 6 shows the pictures of HeLa cells after 24 hours of incubation with different concentrations of magnetite MNPs coated with citric acid. The cells were fixed and stain in order to identify their nucleus and cytoplasm. The aggregates of MNPs appears in the image as brown spots.

It can be observed that the amount of MNPs inside the cells grows with the concentration of the sample employed during incubation. Similar results were observed for the rest of ferrites. Though this kind of microscopies do not guarantee that the MNPs are inside the cells, the stained cells present a higher amount of brown spots than the areas around, suggesting that the cells have internalized a certain amount of them. Further studies are required to confirm the correct internalization of the ferrite MNPs in HeLa cells. The internalization of MNPs of the other ferrites were expected to be similar since they present approximately the same size and the interactions with cell membrane is mediated by the coating.

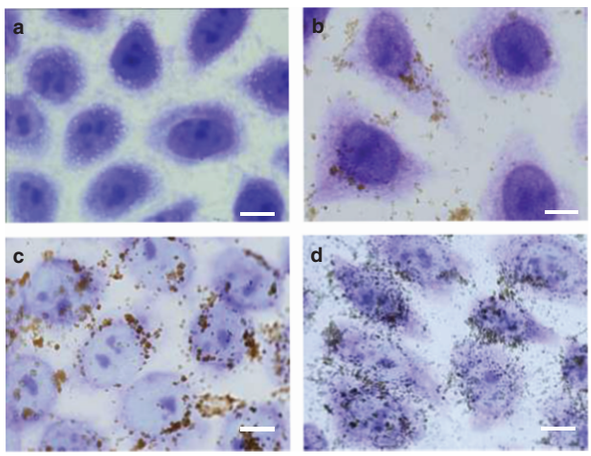

Figure 6. Optical microscopies of HeLa cells incubated with different amount of Fe_3O_4 MNP for 24 hours: (a) Control (0 μg_{Fe}/mL), (b) 10 μg_{Fe}/mL, (c) 50 μg_{Fe}/mL and (d) 100 μg_{Fe}/mL. White scale bar corresponds to 10 μm.

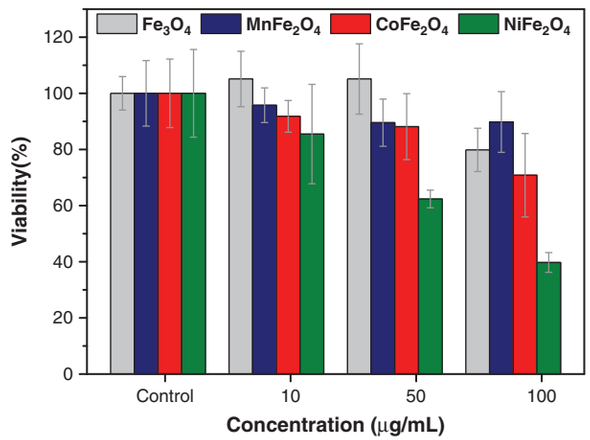

Figure 7. Toxicity analysis by MTT of the different ferrites incubated for 24 hours with the HeLa cell line.

Figure 7 shows the results of the MTT viability assays obtained for the different concentrations and compositions of ferrite MNPs. The concentration was estimated by summing the amount of metallic atoms obtained from ICP-OES measurement. It can be observed that the evolution of the cellular viability with the concentration is different for each ferrite. For magnetite and Mn ferrite, the cellular viability is over 80% for all the analyzed concentrations. In the case of Co ferrite, the viability is lower them in all the cases and falls under 70% for 100 μg/mL. Ni ferrite seems to be the most toxic ferrite with a cellular viability under 40% at the highest concentration studied.

4. CONCLUSIONS

Electrochemical synthesis is an interesting method to produce crystalline MNPs based on quasi-stoichiometric ferrite, in a simple, scalable and water-based way. The magnetic properties of the MNPs produced by this method can be modified by adjusting their composition and size. In order to explain their magnetic behavior, is important to take into account the polydispersity of MNP volume. The cellular viability of HeLa cells incubated with ferrite MNPs depends on the concentration and composition of the sample, being Co and Ni ferrites the most toxic ones for this kind of cells.

Acknowledgment: The authors thank MINECO (Spain) for financial support under project MAT2015-67557-C2-2-P and MAT2015-67557-C2-1-P. Jesus García Ovejero thanks to the MINECO for the FPI scholarship.

References and Notes

1. S. Horikoshi and N. Serpone, Microwaves in Nanoparticle Synthesis, edited by Wiley-VCH Verlag GmbH & Co., KGaA, Weinheim, Germany (**2013**).
2. M. Mohapatra and S. Anand, *Int. J. Eng. Sci. Technol.* 2, 127 (**2011**).
3. P. Li, D. E. Miser, S. Rabiei, R. T. Yadav, and M. R. Hajaligol, *Appl. Catal. B Environ.* 43, 151 (**2003**).
4. Y. Zhang, S. Xu, Y. Luo, S. Pan, H. Ding, and G. Lidoi, *J. Mater. Chem.* 21, 3664 (**2011**).
5. H. Sun, L. Cao, and L. Lu, *Nano Res.* 4, 550 (**2011**).
6. L. Wang, J. Li, Q. Jiang, L. Zhao, K. S. Kim, S. B. Kim, J. X. Zhang, and Y. Z. Chen, *Dalt. Trans.* 41, 4544 (**2012**).
7. H. Graf, J. Vancea, and H. Hoffmann, *Appl. Phys. Lett.* 80, 1264 (**2002**).
8. K. Yakushiji, S. Mitani, K. Takanashi, S. Takahashi, S. Maekawa, H. Imamura, and H. Fujimori, *Appl. Phys. Lett.* 78, 515 (**2001**).
9. A. F. Alves, S. G. Mendo, L. P. Ferreira, M. H. Mendonça, P. Ferreira, M. Godinho, M. M. Cruz, and M. D. Carvalho, *J. Nanoparticle Res.* 18, 27 (**2016**).
10. E. Fantechi, C. Innocenti, M. Albino, E. Lottini, and C. Sangregorio, *J. Magn. Magn. Mater.* 380, 365 (**2015**).
11. T. Kikumori, T. Kobayashi, M. Sawaki, and T. Imai, *Breast Cancer Res. Treat.* 113, 435 (**2009**).
12. J. Dobson, *Drug Dev. Res.* 67, 55 (**2006**).
13. J. Zhang, S. Rana, R. Srivastava, and R. Misra, *Acta Biomater.* 4, 40 (**2008**).
14. D.-B. Shieh, F.-Y. Cheng, C.-H. Su, C.-S. Yeh, M.-T. Wu, Y.-N. Wu, C.-Y. Tsai, C.-L. Wu, D.-H. Chen, and C.-H. Chou, *Biomaterials* 26, 7183 (**2005**).
15. R. Galindo, E. Mazario, S. Gutiérrez, M. P. Morales, and P. Herrasti, *J. Alloys Compd.* 536, S241 (**2012**).
16. A. Akbarzadeh, M. Samiei, and S. Davaran, *Nanoscale Res. Lett.* 7, 144 (**2012**).
17. E. Mazarío, J. Sánchez-Marcos, N. Menéndez, M. Cañete, A. Mayoral, S. Rivera-Fernández, J. M. de la Fuente, and P. Herrasti, *J. Phys. Chem. C* 119, 6828 (**2015**).
18. L. Cabrera, S. Gutierrez, N. Menendez, M. P. Morales, and P. Herrasti, *Electrochim. Acta* 53, 3436 (**2008**).
19. M. Ibrahim, K. G. Serrano, L. Noe, C. Garcia, and M. Verelst, *Electrochim. Acta* 55, 155 (**2009**).
20. D. Ramimoghadam, S. Bagheri, and S. B. A. Hamid, *J. Magn. Magn. Mater.* 368, 207 (**2014**).
21. E. Mazarío, P. Herrasti, M. P. Morales, and N. Menéndez, *Nanotechnology* 23, 355708 (**2012**).
22. D. L. Leslie-Pelecky and R. D. Rieke, *Chem. Mater.* 8, 1970 (**1996**).
23. D. Chen, Q. Tang, X. Li, X. Zhou, J. Zang, J. Xiang, C. Guo, and C. Xue, *Int. J. Nanomedicine* 7, 4973 (**2012**).
24. E. Mazarío, J. Sanchez Marcos, N. Menendez, P. Herrasti, M. García-Hernández, and A. Muñoz Bonilla, *RSC Adv.* 4, 48353 (**2014**).
25. R. A. McCurrie, Ferromagnetic Materials: Structure and Properties, Academic Press, Cop., London (**1994**).
26. J.-H. Lee, Y.-M. Huh, Y. Jun, J. Seo, J. Jang, H.-T. Song, S. Kim, E.-J. Cho, H.-G. Yoon, J.-S. Suh, and J. Cheon, *Nat. Med.* 13, 95 (**2007**).
27. M. Knobel, W. C. Nunes, L. M. Socolovsky, E. De Biasi, J. M. Vargas, and J. C. Denardin, *J. Nanosci. Nanotechnol.* 8, 2836 (**2008**).
28. J. M. D. Coey, Magnetism and Magnetic Materials, Cambridge University Press (**2010**).
29. E. C. Sousa, C. R. Alves, R. Aquino, M. H. Sousa, G. F. Goya, H. R. Rechenberg, F. A. Tourinho, and J. Depeyrot, *J. Magn. Magn. Mater.* 289, 118 (**2005**).
30. O. Moscoso-Londoño, P. Tancredi, D. Muraca, P. Mendoza Zélis, D. Coral, M. B. Fernández van Raap, U. Wolff, V. Neu, C. Damm, C. L. P. de Oliveira, K. R. Pirota, M. Knobel, and L. M. Socolovsky, *J. Magn. Magn. Mater.* 428, 105 (**2017**).

Received: 20 July 2017. Accepted: 1 September 2017.